Lawrence Berkeley National Laboratory

Title

Relativistic Effects on a Metal—Metal Bond: Osmium Corrole Dimers

Permalink

https://escholarship.org/uc/item/9p75z22t

Authors

Alemayehu, Abraham B
McCormick, Laura J
Vazquez-Lima, Hugo
et al.

Relativistic Effects on a Metal−Metal Bond: Osmium Corrole Dimers

Abraham B. Alemayehu,[†] Laura J. McCormick,[‡] Hugo Vazquez-Lima,[†] and Abhik Ghosh*,[†]

[†]Department of Chemistry, UiT − The Arctic University of Norway, N-9037 Tromsø, Norway

[‡]Advanced Light Source, Lawrence Berkeley National Laboratory, Berkeley, California 94720-8229, United States

ABSTRACT: A series of metal−metal bonded osmium corrole dimers, {Os[T*p*XPC]}$_2$, were synthesized in reasonably good yields (35−46%) via the interaction of the corresponding free-base *meso*-tris(*p*-X-phenyl)corroles (H$_3$[T*p*XPC], X = CF$_3$, H, CH$_3$, and OCH$_3$), Os$_3$(CO)$_{12}$, and potassium carbonate in 1,2,4-trichlorobenzene under an inert atmosphere at 180 °C over several hours. The complexes are only the second class of Os corroles reported to date (the first being Os^{VI}N corroles) and also the second class of metal−metal bonded metallocorrole dimers (the other being Ru corrole dimers). Comparison of the X-ray structures, redox potentials, and optical spectra of analogous Ru and Os corrole dimers, along with scalar-relativistic DFT calculations, has provided an experimentally calibrated account of relativistic effects in these complexes. Three of the Os corrole dimers (X = CF$_3$, H, and OCH$_3$) were analyzed with single-crystal X-ray diffraction analysis, revealing inversion-related corrole rings with eclipsed Os−N bonds and Os−Os distances of ∼2.24 Å that are ∼0.06 Å longer than the Ru−Ru distances in the analogous Ru corrole dimers. Interestingly, a comparison of scalar-relativistic and nonrelativistic DFT calculations indicates that this difference in metal−metal bond distance does not, in fact, reflect a differential relativistic effect. For a given corrole ligand, the Ru and Os corrole dimers exhibit nearly identical oxidation potentials but dramatically different reduction potentials, with the Os values ∼0.5 V lower relative to Ru, suggesting that whereas oxidation occurs in a ligand-centered manner, reduction is substantially metal-centered, which indeed was confirmed by scalar-relativistic calculations. The calculations further indicate that approximately a third of the ∼0.5 V difference in reduction potentials can be ascribed to relativity. The somewhat muted value of this relativistic effect appears to be related to the finding that reduction of an Os corrole dimer is not exclusively metal-based but that a significant amount of spin density is delocalized over to the corrole ligand; in contrast, reduction of an Ru corrole dimer occurs exclusively on the Ru−Ru linkage. For isoelectronic complexes, the Ru and Os corrole dimers exhibit substantially different UV−vis spectra. A key difference is a strong near-UV feature of the Os series, which in energy terms is blue-shifted by ∼0.55 V relative to the analogous feature of the Ru series. TDDFT calculations suggest that this difference may be related to higher-energy Os(5d)-based LUMOs in the Os case relative to analogous MOs for Ru.
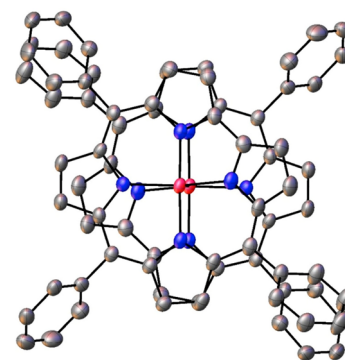
■ INTRODUCTION

It is a matter of common knowledge that second- and third-row transition metals are chemically much more similar to one another than to their first-row counterparts.[1] This similarity is thought to reflect the larger size of the 4d and 5d orbitals of the heavier transition metals relative to the 3d orbitals. The orbital size effect manifests itself in many ways, including the 4d and 5d elements' preference for low-spin states, the ability to adopt higher oxidation states, and the propensity to form metal−metal multiple bonds, relative to the 3d elements. Laboratory researchers concerned with the practicalities of chemical synthesis, however, also tend to be keenly aware of the *differences* between 4d and 5d elements. They may be aware, for example, that the synthesis of analogous 4d and 5d compounds often requires different reaction conditions, such as different reagents and solvents. From a more quantitative perspective, analogous reactions involving 4d and 5d compounds routinely exhibit major differences in kinetic and thermodynamic parameters. Relativistic effects, which significantly destabilize the 5d orbitals of third-row transition elements relative to the 4d orbitals of second-row transition elements, are thought to account for a significant fraction of these differences.[2,3] Herein, using isoelectronic, structurally characterized ruthenium and osmium corrole dimers as paradigms, we present a study of relativistic effects on metal−metal multiple bonds.

The relativistic effect (ΔP) on a molecular property P, such as an ionization potential or a bond distance, is defined as the difference between relativistic (P$_{rel}$) and nonrelativistic (P$_{nrel}$) calculated values of that property. Relativistic effects, accordingly, are purely theoretical quantities. For ΔP to be meaningful in a practical sense, however, we need to ensure that P$_{rel}$ is calculated at a high enough level so that it matches the experimental value of the property P$_{expt}$ and that P$_{nrel}$ is calculated at essentially the same theoretical level except for the relativistic treatment. Under these conditions, i.e., P$_{expt}$ = P$_{nrel}$, we may with some justification speak about the relativistic effect on an experimentally determined property P$_{expt}$ or, more briefly, an experimentally calibrated relativistic effect. For-

tunately, density functional theory (DFT) often provides both a computationally expedient and a surprisingly accurate description of relativistic effects on heavy element compounds.[4−11]

We hypothesized that 5d−5d multiple bonds should provide particularly good examples of strong relativistic effects. Since Ru corrole dimers are already known,[12−15] Os corrole dimers appeared to be logical targets for synthesis and detailed characterization. Moreover, Os corrole chemistry is still in its infancy, with $Os^{VI}N$ corroles as the only known representatives.[16] Like certain other 5d metallocorroles,[17−21] $Os^{VI}N$ corroles also exhibit near-IR phosphorescence and have been applied as optical sensors for oxygen and as sensitizers for triplet−triplet annihilation upconversion.[22] Thus motivated, we duly synthesized a series of Os corrole dimers. Comparison with the analogous Ru compounds indeed revealed substantial relativistic effects for the Os series.

■ RESULTS AND DISCUSSION

Synthesis and Proof of Composition. Two isoelectronic series of metal−metal−bonded dimers, $\{M[TpXPC]\}_2$, were prepared, where M = Ru and Os and $H_3[TpXPC]$ refers to a free-base *meso*-tris(*p*-X-phenyl)corroles ($H_3[TpXPC]$, X = CF_3, H, CH_3, and OCH_3). The Ru series could be accessed via minor modification of an existing synthetic protocol, namely from free-base corroles and $[Ru(cod)Cl_2]_x$ in refluxing 2-methoxyethanol in the presence of an amine base.[12−14] A new protocol, however, had to be developed for the Os dimers, which in its final, optimized form involved the interaction of a free-base corrole, $Os_3(CO)_{12}$, and potassium carbonate in 1,2,4-trichlorobenzene under an inert atmosphere at 180 °C over ~16 h (Figure 1). Upon completion of the reaction (as
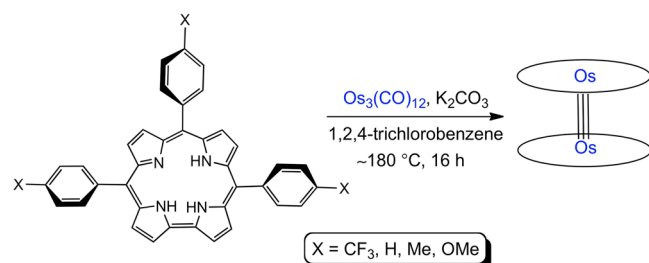

Figure 1. Synthesis of Os corrole dimers.

indicated by UV−vis spectroscopy), high-resolution electrospray ionization mass spectrometric analysis indicated the formation of Os corrole dimers. Upon cooling, the reaction mixture was subjected to column chromatography, affording the desired complexes as reddish-brown solids in 35−46% yields.

The complexes yielded broad ^1H NMR spectra at room temperature, but the spectra sharpened significantly at 253 K (Figure 2), clearly indicating the compounds as diamagnetic. The diamagnetism of the compounds is consistent with Cotton's molecular orbital (MO) model of d−d metal−metal bonding,[23] which predicts an Os−Os triple bond with a $\sigma^2\pi^4\delta^2\delta^{*2}$ configuration. It may be recalled that the analogous Group 8 metal−metal−bonded porphyrins are paramagnetic, triplet species with a $\sigma^2\pi^4\delta^2\delta^{*2}\pi^{*2}$ configuration.[24−26] The ^1H NMR spectra at 253 K could be essentially fully assigned, revealing symmetry-related *meso*-triarylcorrole ligands in which the *ortho* and *meta* protons of each phenyl ring are split into

symmetry-distinct pairs; the latter feature is typical for square-pyramidally coordinated corrole derivatives.[27]

X-ray Crystal Structures. Conclusive proof of structure came from three single-crystal X-ray structures, as detailed in Tables 1 and 2 and Figure 3. All three structures are characterized by approximately inversion-related corrole rings and approximately eclipsed Os−N bonds. Such a conformation allows for δ-bonding between the $Os(d_{xy})$ orbitals and also minimizes steric repulsions among the phenyl substituents. The three structures also exhibit mutually consistent Os−N (1.95 ± 0.05 Å) and Os−Os (~2.24 Å) distances and Os−N_{plane} displacements (~0.51 Å). Interestingly, while the M−N and M−N_{plane} distances are nearly identical for Ru and Os corrole dimers, the Os−Os distances are significantly longer than the Ru−Ru distances (~2.18 Å, Table 2). An interesting question concerns to what extent these metal−metal bond distances are affected by relativistic effects. $B3LYP^{28−30}$-$D3^{31}$/ STO-TZP geometry optimizations of $\{Os[TPC]\}_2$ with nonrelativistic and zeroth order regular approximation $(ZORA)^{32,33}$ scalar-relativistic Hamiltonians yielded very similar Os−Os distances, 2.255 and 2.262 Å, respectively. The limited amount of computational data in the literature also suggests that relativistic effects should only have a minor influence on 4d−4d and 5d−5d metal−metal bonds.[34−37]

Electrochemistry. The cyclic voltammograms of both the Ru and Os corrole dimers exhibit at least three reversible oxidations and two reversible reductions (Table 3 and Figure 4). The oxidation potentials $E_{1/2ox1}$ through $E_{1/2ox3}$ turned out to be very similar for the Ru and Os dimers, as expected for ligand-centered processes. The reduction potentials, on the other hand, were found to be dramatically lower for the Os series (i.e., they are harder to reduce), downshifted by essentially 0.5 V relative to the Ru series, strongly implicating the metal centers as the site of reduction. Essentially the same downshift is also observed for the oxidation potentials of Os porphyrin dimers (i.e., they are easier to oxidize) relative to their ruthenium counterparts.[24−26] The question thus arises as to what fraction of this downshift is attributable to differences in relativistic effects for the two metals.

B3LYP-D3/STO-TZP calculations of the adiabatic ionization potentials of $\{Ru[TPC]\}_2$ and $\{Os[TPC]\}_2$ yielded nearly identical values of 5.40 ± 0.05 eV, regardless of relativistic treatment, consistent with ligand-centered ionization, as surmised above. The adiabatic electron affinities of the two complexes, in contrast, proved to be significantly different at both the nonrelativistic and scalar-relativistic levels. With a nonrelativistic Hamiltonian, the adiabatic EAs turned out to be 2.642 eV for $\{Ru[TPC]\}_2$ and 2.368 eV for $\{Os[TPC]\}_2$. With ZORA applied as a scalar approximation, the relativistic adiabatic EAs turned out to be 2.501 eV for $\{Ru[TPC]\}_2$ and 1.957 eV for $\{Os[TPC]\}_2$. Key lessons from these results include the following: The relativistic effect on the adiabatic EA is significant for $\{Ru[TPC]\}_2$ (0.14 eV) but nearly three times higher for $\{Os[TPC]\}_2$ (0.41 eV). Second, even at the nonrelativistic level, the adiabatic EA of $\{Os[TPC]\}_2$ is 0.27 eV lower than that of $\{Ru[TPC]\}_2$, but the difference increases to just over 0.40 eV at the relativistic level, in fair agreement with the difference in experimental reduction potentials of the two compounds. The results suggest that about a third of the difference in reduction potentials between Ru and Os may be attributed to differential relativistic effects between the two elements. Based on comparative electrochemical measurements of Mo and W biscorrole sandwich compounds,[38−40]
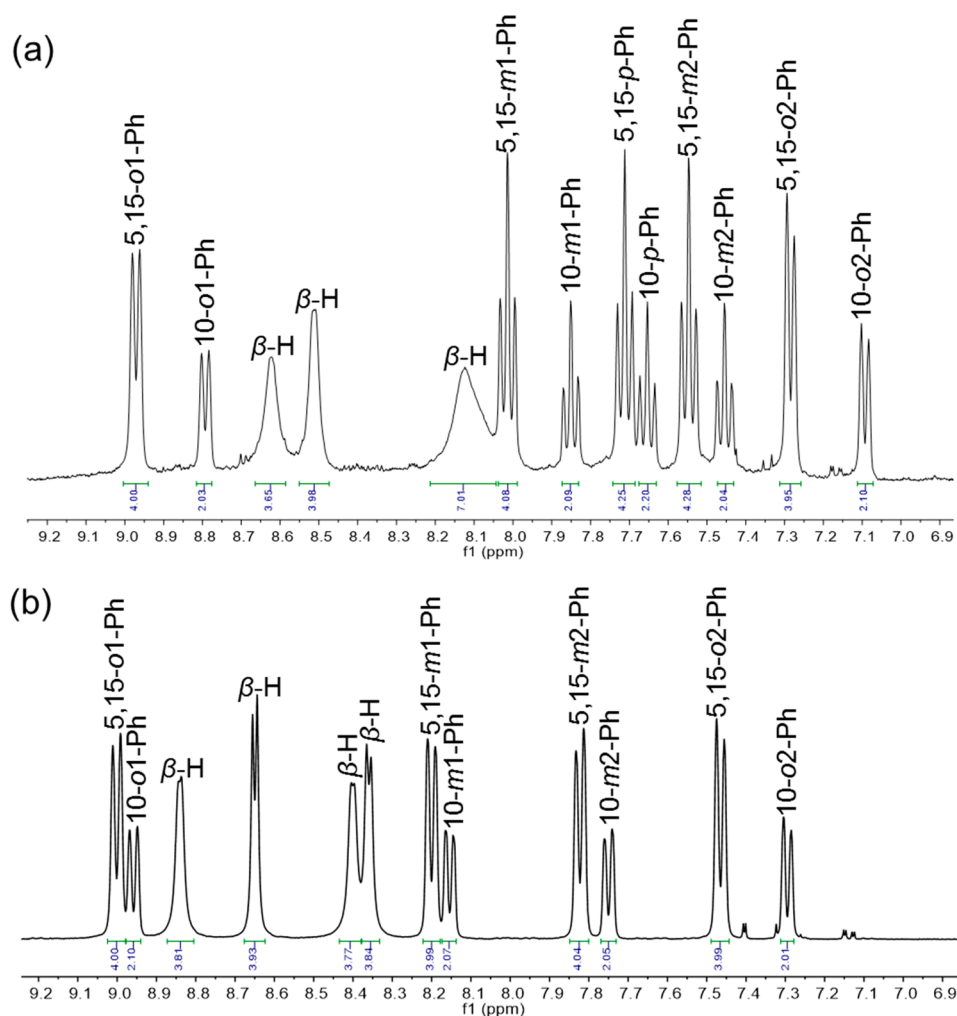
Figure 2. Representative ^{1}H NMR spectra in CD_2Cl_2 at 253 K: (a) {Os[TPC]}$_2$ and (b) {Os[TpCF$_3$PC]}$_2$.

however, we expected a somewhat larger relativistic effect for the reduction potential of {Os[TPC]}$_2$ as well as for the differential relativistic effect between {Ru[TPC]}$_2$ and {Os-[TPC]}$_2$. An examination of the scalar-relativistic spin density profiles of the ionized states of the two complexes provided a plausible explanation for the somewhat muted relativistic effect in the Os case (Figure 5).

For the cationic states of both {Ru[TPC]}$_2$ and {Os-[TPC]}$_2$, the spin density was found to be entirely localized on the ligands, in agreement with the discussion above. The spin density corresponds to electron removal from a corrole "a$_{2u}$"-based HOMO of the dimeric molecules, permitting ourselves to use the D_{4h} irreducible representation that is appropriate for the analogous porphyrin HOMO. For {Ru[TPC]}$_2$ anion, on the other hand, the spin density is largely (∼80%) localized on the Ru atoms, consistent with single occupancy of one of the Ru−Ru π*-based MOs, which accounts for the significant relativistic effect on the EA. For {Os[TPC]}$_2$ anion, in contrast, the spin density is split approximately 1:1 between the Os$_2$ moiety and the TPC ligands. The relativistically elevated energy of the Os(5d) orbitals apparently pushes part of the spin density over to a corrole-based MO of the appropriate symmetry, as qualitatively illustrated by the LUMO of {Os[TPC]}$_2$ (Figure 5). The finding that one-electron reduction does not occur in a predominantly metal-centered manner nicely explains why the relativistic effect on

the reduction potential of {Os[TPC]}$_2$, while substantial, is not quite as dramatic as might have been anticipated.

UV−Visible Spectroscopy. For isoelectronic compounds, the {Ru[TpXPC]}$_2$ and {Os[TpXPC]}$_2$ series exhibit remarkably different UV−vis spectra (Figure 6). In our earlier work on metallocorroles, we have regularly used different *para*-X-substituted corrole derivatives as a probe for a noninnocent corrole ligand, which almost invariably manifests itself as a substituent-sensitive Soret maximum.[41] By this criterion, the Ru and Os corrole dimers, like the majority of 4d and 5d metallocorroles (including MoO,[42] RuN,[14] OsN,[16] TcO,[43] ReO,[44] Pt,[45] and Au[46−49] corroles), appear to be innocent. The spectra of both series of dimers are nonetheless unusual, relative to first-row transition metal corroles, and are characterized by intense near-UV features. Thus, both the Ru and Os series exhibit Soret-like bands at ∼400 nm and intense higher-energy "post-Soret" bands. The latter feature occurs at ∼328 nm for the Ru series and at ∼287 nm for the Os series, which corresponds to an energy difference of ∼0.55 eV. In addition, the Os series exhibits a third well-resolved peak in the near-UV region at ∼363 nm. The Ru series also exhibits a well-resolved Q-band at 537 ± 4 nm, which appears to exhibit slight substituent dependence, while the Q bands of the Os series only appear as a less distinct feature at around 590 nm.

Table 1. Crystallographic Data for the Complexes Analyzed

Sample	$\{Os[TpCF_3C]\}_2$	$\{Os[TPC]\}_2$	$\{Os[TpOMeC]\}_2$
Chemical formula	$C_{92}H_{68}F_{18}N_8Os_2$	$C_{148}H_{92}N_{16}Os_{3.41}$	$C_{80}H_{58}N_8O_6Os_2$
Formula mass	2007.94	2743.66	1607.74
Crystal system	Triclinic	Triclinic	Triclinic
Crystal size (mm^3)	$0.270 \times 0.080 \times 0.005$	$0.150 \times 0.050 \times 0.010$	$0.140 \times 0.020 \times 0.010$
Space group	$P\bar{1}$	$P\bar{1}$	$P\bar{1}$
λ (Å)	0.7749	0.7749	0.8856
a (Å)	9.625(3)	12.8033(7)	11.4553(6)
b (Å)	15.330(5)	13.0678(7)	12.4466(7)
c (Å)	16.018(6)	17.0021(9)	12.9535(8)
α (deg)	111.503(7)	101.482(2)	71.171(4)
β (deg)	96.578(7)	101.895(2)	80.750(4)
γ (deg)	101.453(7)	105.645(2)°	83.551(4)
Z	1	1	1
V (Å^3)	2109.1(13)	2580.7(2)	1721.72(18)
Temperature (K)	100(2)	100(2)	100(2)
Density (g/cm^3)	1.581	1.765	1.551
Measured reflections	81222	68853	9809
Unique reflections	8595	10596	4483
Parameters	596	661	442
Restraints	116	9	232
R_{int}	0.0581	0.0407	0.0682
θ range (deg.)	1.522−28.999	1.833−29.018	2.159−28.520
R_1, wR_2 all data	0.0418, 0.1062	0.0408, 0.1045	0.1088, 0.1642
S (GooF) all data	1.069	1.083	1.054
Max/min res. dens. (e/Å^3)	2.612/-1.672	3.140/-1.431	2.524/-1.148

Table 2. Selected Crystallographic Distances (Å) Relevant to the Osmium Coordination Geometry

Complex	Os−N1	Os−N2	Os−N3	Os−N4	Os−Os	Os−N$_{plane}$
$\{Os[TpCF_3C]\}_2$	1.979(4)	2.002(4)	1.991(4)	1.977(4)	2.2398(7)	0.522(2)
$\{Os[TPC]\}_2$	1.959(4)	1.979(4)	1.978(4)	1.968(4)	2.2346(4)	0.507(2)
	1.961(6)	1.960(7)	1.963(6)	1.951(7)	2.2403(5)	0.519(3)
$\{Os[TpOMeC]\}_2$	1.910(16)	1.979(12)	1.945(14)	1.959(12)	2.2291(13)	−0.510(5)
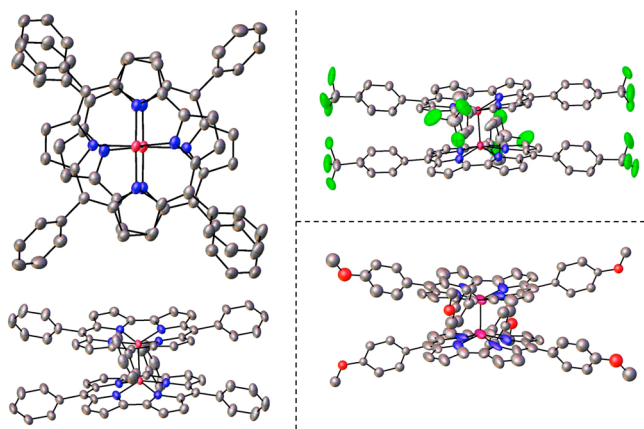
Figure 3. Thermal ellipsoid plots (50%) for $\{Os[TPC]\}_2$ (left), $\{Os[TpCF_3C]\}_2$ (top right), and $\{Os[TpOCH_3C]\}_2$ (bottom right).

Scalar-relativistic time-dependent density functional theory (TDDFT; B3LYP-D3/ZORA-STO-TZP) calculations do a rather good job of reproducing key features of the UV−vis spectra of $\{Ru[TPC]\}_2$ and $\{Os[TPC]\}_2$, including the blue-shifted post-Soret feature of the latter (Figure 7). A detailed discussion of peak assignments, however, is impractical, not only because of the large number of transitions within a given spectral region but also because of the multiplicity of individual MO-to-MO excitations contributing to each transition. The relativistic MO energy levels of the two compounds, however, readily permit a discussion of relativistic effects. There is little difference in the orbital energy levels for the few highest occupied MOs of the two complexes, which consist of combinations of the Gouterman-type HOMOs of the two corroles.[50,51] Likewise, purely Gouterman-type LUMOs have similar orbital energies for the two molecules. On the other hand, LUMOs with significant or predominant metal d character are destabilized in $\{Os[TPC]\}_2$ by as much 0.5−1.0 eV, relative to $\{Ru[TPC]\}_2$. Comparison with an analogous nonrelativistic MO energy level diagram (not shown) showed that the differences between Ru and Os energy levels are largely attributable to much stronger relativistic effects for Os 5d orbitals. A detailed examination of the MO-to-MO composition of the transitions in different spectral regions further confirmed that relativistically destabilized Os 5d-based MOs indeed account for much of the intensity of the unique, blue-shifted post-Soret peak of $\{Os[TPC]\}_2$.

■ CONCLUSION

The 4d and 5d metallocorroles are a novel class of size-mismatched complexes incorporating a large transition metal ion within the sterically constrained N_4 cavity of a corrole. The metal insertion process is almost invariably capricious, requiring specific reagents, solvents, and temperatures, but

Table 3. Optical Spectroscopic and Electrochemical Properties of $\{Ru[TpXPC]\}_2$ and $\{Os[TpXPC]\}_2$: λ_{max} (nm) for Soret and Q Bands and $E_{1/2}$ Values (V)

| Complex	λ_{max}	Q	$E_{1/2ox4}$	$E_{1/2ox3}$	$E_{1/2ox2}$	$E_{1/2ox1}$	$E_{1/2red1}$	$E_{1/2red2}$	ΔE
$\{Ru[TpCF_3PC]\}_2$	328, 397	541		1.31	1.09	0.76	−0.63	−1.43	1.39
$\{Ru[TPC]\}_2$	328, 397	539	1.56	1.23	0.99	0.55	−0.86	−1.66	1.41
$\{Ru[TpCH_3PC]\}_2$	329, 398	538	1.44	1.18	0.98	0.52	−0.85		1.37
$\{Ru[TpOCH_3PC]\}_2$	329, 406	533	1.33	1.14	0.92	0.50	−0.86		1.36
$\{Os[TpCF_3PC]\}_2$	287, 407	583		1.28	1.01	0.79	−1.13	−1.54	1.92
$\{Os[TPC]\}_2$	287, 405	584		1.15	0.93	0.60	−1.29	−1.69	1.89
$\{Os[TpCH_3PC]\}_2$	287, 407	584	1.35	1.09	0.88	0.55	−1.31	−1.72	1.86
$\{Os[TpOCH_3PC]\}_2$	286, 407	585	1.28	1.05	0.85	0.54	−1.32	−1.73	1.86
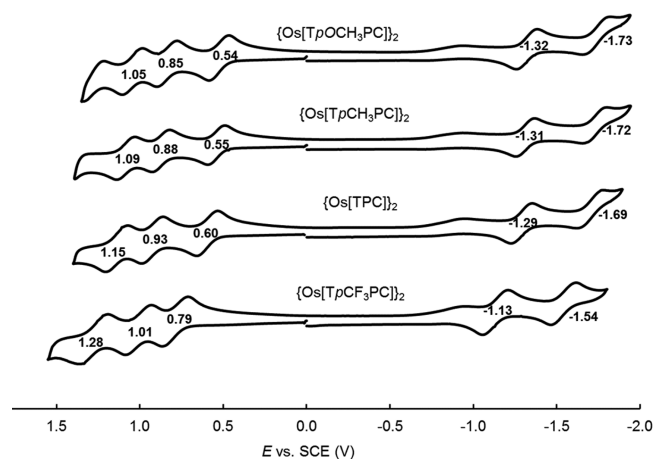
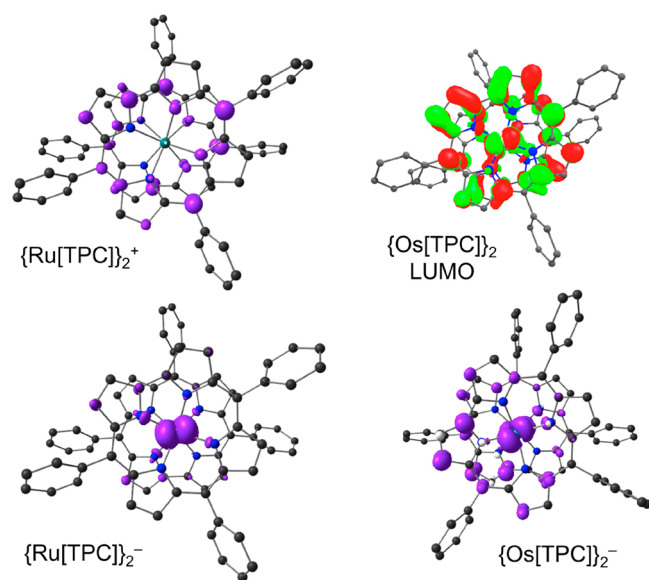Figure 4. Cyclic voltammograms of $\{Os[TpXPC]\}_2$ in dichloromethane containing 0.1 M TBAP.

Figure 5. Selected scalar relativistic B3LYP-D3/ZORA-STO-TZP spin density and MO plots.

Figure 6. UV−vis spectra of (a) $\{Os[TpXPC]\}_2$ and (b) $\{Ru[TpXPC]\}_2$ in dichloromethane.

the products, once formed, are often stable, potentially allowing for a wide range of applications. Against this backdrop, we have presented the synthesis of osmium corrole dimers, which are only the second class of Os corrole derivatives ever to be reported. The compounds were obtained in fairly good yields, 35−46%, which are roughly double those obtained for analogous Ru corrole dimers. Whether the new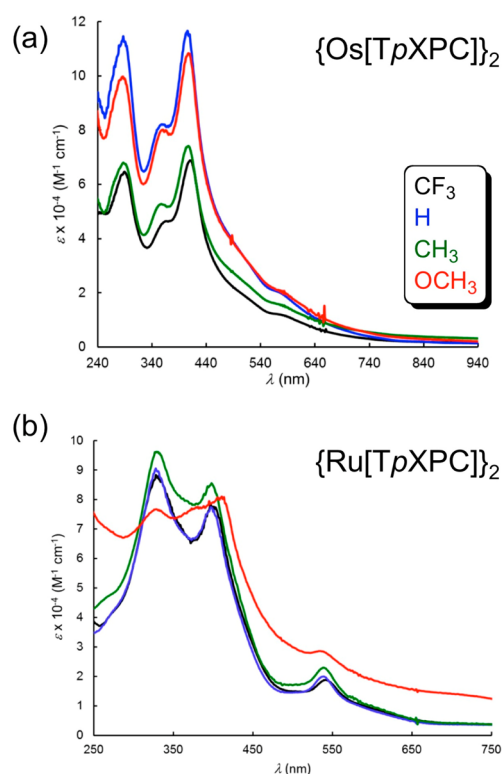 compounds prove amenable to reductive cleavage and thereby serve as a source of new mononuclear Os corrole complexes remains an exciting prospect for the future.

Analogous Ru and Os corrole dimers have permitted a detailed study of experimentally calibrated relativistic effects on Group 8 metallocorroles. Single-crystal X-ray structures of three Os corrole dimers revealed Os−Os distances of ∼2.24 Å, which are ∼0.06 Å longer than the Ru−Ru distances in analogous Ru corrole dimers. Interestingly, DFT geometry optimizations with scalar-relativistic and nonrelativistic Hamiltonians revealed an almost vanishingly small relativistic effect on these distances.

The redox potentials of the compounds and associated calculations on the gas-phase ionization potentials and electron affinities of the compounds provided some of the most significant insights into relativistic effects on the compounds. For a given corrole ligand, the Ru and Os dimers were found to exhibit very similar oxidation potentials, consistent with ligand-centered oxidation; the Os dimers on the other hand were found to exhibit substantially lower reduction potentials, by a margin of 0.5 eV, suggesting reduction of the metal−metal
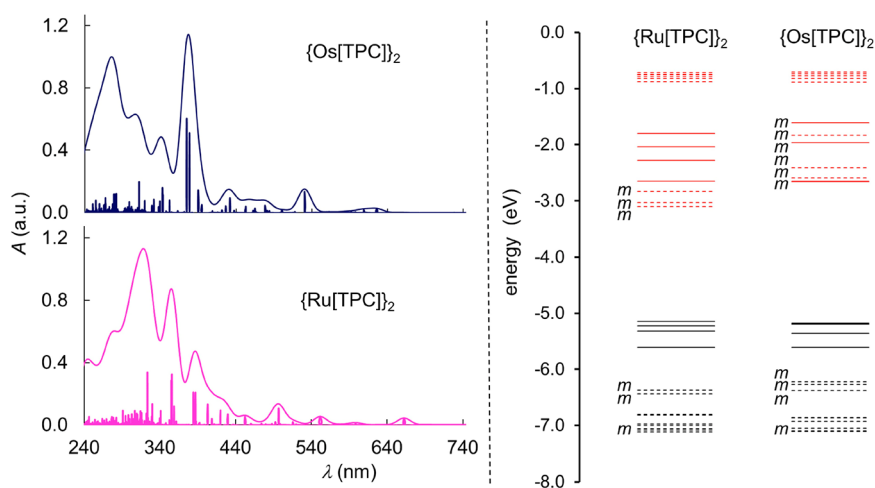
Figure 7. Left: Scalar-relativistic ZORA-TDDFT (B3LYP-D3/STO-TZP) simulated spectra for {Ru[TPC]}$_2$ and {Os[TPC]}$_2$ (left) and the corresponding Kohn–Sham energy level diagrams (right). Solid and dotted lines indicate Gouterman-type and other MOs, respectively, while the label *m* denotes greater than 20% metal character.

bond. Gas-phase scalar-relativistic DFT calculations of ionization potentials and electron affinities nicely reproduced the trends in electrochemical data. In particular, the calculations suggested that about a third of the difference in reduction potential between analogous Ru and Os corrole dimers can be attributed to relativistic effects, which is somewhat smaller than what we expected. A plausible explanation is provided by scalar-relativistic spin density profiles, which indicate that one-electron reduction of the Os dimer does not occur exclusively on the metal−metal bond, but that as much as half the spin density is delocalized onto the corrole rings.

The Ru and Os corrole dimers exhibit significantly different electronic absorption spectra in the UV−vis regime, including an intense post-Soret feature in the case of the Os compounds that is some 0.55 eV blue-shifted relative to the analogous feature for the Ru compounds. TDDFT calculations suggest that a large number of the transitions in this region have metal d-based LUMO character, which leads to a higher transition energy in the Os case, as a result of strong relativistic destabilization of the Os(5d) orbitals.

■ EXPERIMENTAL SECTION

Materials. All free-base corroles were synthesized via the now-standard water−methanol method.[52] The reagents 1,2,4-trichlorobenzene, triosmium dodecacarbonyl (99.99%), potassium carbonate (granulated), 2-methoxyethanol, trimethylamine, and (1,5-cyclooctadiene)ruthenium(II) polymer were purchased from Sigma-Aldrich and used as received. Silica gel 60 (0.04−0.063 mm particle size, 230−400 mesh, Merck) was employed for flash chromatography. Silica gel 60 preparative thin-layer chromatographic plates (20 cm × 20 cm × 0.5 mm, Merck) were used for final purification of all complexes.

General Instrumental Methods. UV−visible spectra were recorded on an HP 8453 spectrophotometer. ^{1}H NMR spectra (253 K, CD$_2$Cl$_2$) were recorded on a 400 MHz Bruker Avance III HD spectrometer equipped with a 5 mm BB/1H SmartProbe and referenced to residual CH$_2$Cl$_2$ at 5.31 ppm. High-resolution electrospray-ionization (HR-ESI) mass spectra were recorded on an LTQ Orbitrap XL spectrometer, using methanolic solutions and typically in positive ion mode. Elemental analyses were performed by Atlantic Microlab Inc., U.S.A.[53]

Cyclic voltammetry was carried out at 298 K with an EG&G Model 263A potentiostat equipped with a three-electrode system: a glassy carbon working electrode, a platinum wire counterelectrode, and a saturated calomel reference electrode (SCE). Tetra(*n*-butyl)-ammonium perchlorate, recrystallized twice from absolute ethanol and dried in a desiccator for at least 2 weeks, was used as the supporting electrolyte. Anhydrous CH$_2$Cl$_2$ (Aldrich) was used as solvent. The reference electrode was separated from the bulk solution by a fritted-glass bridge filled with the solvent/supporting electrolyte mixture. The electrolyte solution was purged with argon for at least 2 min prior to all measurements, which were carried out under an argon blanket. All potentials were referenced to the SCE.

General Procedure for the Synthesis of {Ru[T*p*XPC]}$_2$. To a solution of the free-base corrole, H$_3$[T*p*XPC] (0.136 mmol), in refluxing 2-methoxyethanol (10 mL) under argon, was added trimethylamine (50 μL), followed by {Ru(cod)Cl$_2$}$_x$ (115 mg, 0.41 mmol). After stirring for 30 min, the reaction mixture was cooled to room temperature, the solvent was evaporated, and the resulting crude solid was purified by column chromatography on silica gel with 3:2 dichloromethane/hexane as eluent. For final characterization, the product was further purified by preparative thin-layer chromatography on silica gel with 3:1 dichloromethane/hexane as eluent.

*{Ru[T*p*CF$_3$PC]}$_2$.* Yield 20.2 mg (0.0122 mmol, 17.9%). UV−vis (CH$_2$Cl$_2$) λ_{max} (nm) and ε x 10^{-4} (M^{-1}cm^{-1}): 328 (8.83), 397 (7.82), 541(1.88). ^{1}H NMR (400 MHz, − 20 °C): δ 9.10 (d, 2H, $^3J_{HH}$ = 8.0 Hz, 10-*o*1-Ph); 8.99 (d, 4H, $^3J_{HH}$ = 8.0 Hz, 5,15-*o*1-Ph); 8.83 (d, 4H, $^3J_{HH}$ = 3.5 Hz, β-H); 8.66 (d, 4H, $^3J_{HH}$ = 4.2 Hz, β-H); 8.35 (bs, 8H, β-H); 8.15 (overlapping d, 6H, $^3J_{HH}$ = 9.5 Hz, 10-*m*1-Ph and 5,15-*m*1-Ph); 7.86 (d, 4H, $^3J_{HH}$ = 8.0 Hz, 5,15-*o*2-Ph); 7.80 (d, 2H, $^3J_{HH}$ = 8.5 Hz, 10-*o*2-Ph); 7.53 (d, 4H, $^3J_{HH}$ = 8.0 Hz, 5,15-*m*2-Ph); 7.37 (d, 2H, $^3J_{HH}$ = 7.7 Hz, 10-*m*2-Ph). HRMS (ESI): M$^+$ = 1658.1185 (expt), 1658.1202 (calcd for C$_{80}$H$_{40}$F$_{18}$N$_8$Ru$_2$, major isotopomer). Elemental analysis (%): found C 57.69, H 2.62, N 6.32; calcd C 57.98, H 2.43, N 6.76.

{Ru[TPC]}$_2$. Yield 15.0 mg (0.0119 mmol, 17.6%). UV−vis (CH$_2$Cl$_2$) λ_{max} (nm) and ε x 10^{-4} (M^{-1}cm^{-1}): 328 (9.06), 397 (7.74), 539 (1.99). ^{1}H NMR (400 MHz, − 20 °C): δ 9.05 (d, 4H, $^3J_{HH}$ = 7.2 Hz, 5,15-*o*1-Ph); 8.93 (d, 2H, $^3J_{HH}$ = 8.2 Hz, 10-*o*1-Ph); 8.77 (bs, 4H, β-H); 8.60 (bs, 4H, β-H); 8.29 (bs, 8H, β-H); 7.99 (t, 4H, $^3J_{HH}$ = 7.2 Hz, 5,15-*m*1-Ph); 7.82 (t, 2H, $^3J_{HH}$ = 7.2 Hz, 10-*m*1-Ph); 7.75 (t, 4H, $^3J_{HH}$ = 7.2 Hz, 5,15-*p*-Ph); 7.69 (t, 2H, $^3J_{HH}$ = 7.2 Hz, 10-*p*-Ph); 7.55 (t, 4H, $^3J_{HH}$ = 7.2 Hz, 5,15-*m*2-Ph); 7.45 (t, 2H, $^3J_{HH}$ = 7.2 Hz, 10-*m*2-Ph); 7.33 (d, 4H, $^3J_{HH}$ = 8.2 Hz, 5,15-*o*2-Ph); 7.13 (d, 2H, $^3J_{HH}$ = 7.2 Hz, 10-*m*2-Ph). HRMS (ESI): M$^+$ = 1250.2009 (expt), 1250.1986 (calcd for C$_{74}$H$_{46}$N$_8$Ru$_2$, major isotopomer). Elemental analysis (%): found C 70.85, H 3.49, N 8.62; calcd C 71.14, H 3.71, N 8.97.

{Ru[TpCH₃PC]}₂. Yield 17.25 mg (0.0129 mmol, 19.0%). UV−vis (CH$_2$Cl$_2$) λ_{max} (nm) and ε x 10^{-4} (M^{-1}cm^{-1}): 329 (9.61), 398 (8.54), 538(2.29). ^{1}H NMR (400 MHz, − 20 °C): δ 8.83 (d, 4H, $^3J_{HH}$ = 8.44 Hz, 5,15-*o*1-Ph); 8.67 (d, 2H, $^3J_{HH}$ = 7.48 Hz, 10-*o*-Ph); 8.45 (bs, 4H, β-H); 8.32 (bs, 4H, β-H); 7.89 (d, 4H, $^3J_{HH}$ = 7.48 Hz, 5,15-*m*1-Ph); 7.80 (bs, 8H, β-H); 7.71(d, 2H, $^3J_{HH}$ = 7.48 Hz, 10-*m*1-Ph); 7.45 (d, 4H, $^3J_{HH}$ = 8.48 Hz, 5,15-*o*2-Ph); 7.34 (d, 2H, $^3J_{HH}$ = 8.44 Hz, 10-*o*2-Ph); 7.15 (d, 4H, $^3J_{HH}$ = 7.72 Hz, 5,15-*m*2-Ph); 6.93 (d, 2H, $^3J_{HH}$ = 8.44 Hz, 10-*m*2-Ph); 2.82 (s, 12H, 5,15-*p*-CH$_3$); 2.76 (s, 6H, 10-*p*-CH$_3$). HRMS (ESI): M$^+$ = 1334.2867 (expt), 1334.2903 (calcd for C$_{80}$H$_{58}$N$_8$Ru$_2$, major isotopomer). Elemental analysis (%): found C 70.12, H 4.98, N 7.84; calcd: C 72.05, H 4.38, N 8.40.

{Ru[TpOCH₃PC]}₂. Yield 15.3 mg (0.0106 mmol, 15.7%). UV−vis (CH$_2$Cl$_2$) λ_{max} (nm) and ε x 10^{-4} (M^{-1}cm^{-1}): 329 (7.66), 406 (8.06), 533(2.85). ^{1}H NMR (400 MHz, − 20 °C): δ 8.88 (d, 4H, $^3J_{HH}$ = 8.08 Hz, 5,15-*o*1-Ph); 8.86 (d, 2H, $^3J_{HH}$ = 8.92 Hz, 10-*o*1-Ph); 8.69 (d, 4H, $^3J_{HH}$ = 3.88 Hz, β-H); 8.58 (d, 4H, $^3J_{HH}$ = 3.88 Hz, 5,15-*m*1-Ph); 8.22 (bs, 8H, β-H); 7.52 (d, 4H, $^3J_{HH}$ = 8.08 Hz, 5,15-*m*1-Ph); 7.42(d, 2H, $^3J_{HH}$ = 8.08 Hz, 10-*m*1-Ph); 7.26 (d, 4H, $^3J_{HH}$ = 8.08 Hz, 5,15-*o*2-Ph); 7.09 (d, 4H, $^3J_{HH}$ = 8.64 Hz, 5,15-*m*2-Ph); 7.07 (d, 2H, $^3J_{HH}$ = 8.04 Hz, 10-*o*2-Ph); 7.01 (d, 2H, $^3J_{HH}$ = 8.44 Hz, 10-*m*2-Ph); 4.10 (s, 12H, 5,15-*p*-OCH$_3$); 4.07 (s, 6H, 10-*p*-OCH$_3$). HRMS (ESI): M$^+$ = 1430.2481 (expt), 1430.2445 (calcd for C$_{80}$H$_{58}$N$_8$O$_6$Ru$_2$, major isotopomer). Elemental analysis (%): found C 65.07, H 5.47, N 6.41; calcd C 67.22, H 4.09, N 7.84.

General Procedure for the Synthesis of {Os[T*p*XPC]}₂. A two-necked 50 mL round-bottom flask was charged with free-base corrole, H$_3$[T*p*XPC] (0.109 mmol), Os$_3$(CO)$_{12}$ (0.109 mmol, 98.75 mg), potassium carbonate (100 mg), 1,2,4-trichlorobenzene (10 mL), and a stirring bar. The contents were deoxygenated with a constant flow of argon for 10 min and then heated (180 °C) overnight with constant stirring under Ar. Completion of the reaction was indicated by the disappearance of the Soret absorption band of the free-base corrole and appearance of a new split Soret band with maxima at approximately 287 and 407 nm. Upon cooling, the reaction mixture was loaded directly onto a silica gel column with *n*-hexane as the mobile phase. 1,2,4-Trichlorobenzene was first removed by eluting with pure hexane. *n*-Hexane/dichloromethane (1:3) mixtures were then used to elute the reddish-brown Os corrole dimer. Subsequent preparative thin-layer chromatography with 1:3 hexane/dichloromethane resulted in final yields of 35−46%. Analytical details for the Os corrole dimers are given below.

{Os[TpCF₃PC]}₂. Yield 35.0 mg (0.019 mmol, 35.0%). UV−vis (CH$_2$Cl$_2$) λ_{max} (nm) and ε x 10^{-4} (M^{-1}cm^{-1}): 287 (6.46), 363 (4.65), 407 (6.88), 583 (1.17). ^{1}H NMR (400 MHz, − 20 °C): δ 9.05 (d, 4H, $^3J_{HH}$ = 7.88 Hz, 5,15-*o*1-Ph); 9.00 (d, 2H, $^3J_{HH}$ = 7.36 Hz, 10-*o*1-Ph); 8.88 (bs, 4H, β-H); 8.69 (d, 4H, $^3J_{HH}$ = 5.08 Hz, β-H); 8.45 (bs, 4H, β-H); 8.40 (d, 4H, $^3J_{HH}$ = 4.32 Hz, β-H); 8.25 (d, 4H, $^3J_{HH}$ = 7.36 Hz, 5,15-*m*1-Ph); 8.20 (d, 2H, $^3J_{HH}$ = 8.12 Hz, 10-*m*1-Ph); 7.87 (d, 4H, $^3J_{HH}$ = 7.88 Hz, 5,15-*m*2-Ph); 7.79 (d, 2H, $^3J_{HH}$ = 8.60 Hz, 10-*m*2-Ph); 7.51 (d, 4H, $^3J_{HH}$ = 7.36 Hz, 5,15-*o*2-Ph); 7.34 (d, 2H, $^3J_{HH}$ = 8.12 Hz, 10-*o*2-Ph); ^{13}C NMR (100 MHz, CD$_2$Cl$_2$): δ 29.82, 115.84, 117.26, 118.03, 123.56, 124.15, 124.36, 124.61, 125.03, 125.34, 126.24, 126.96, 128.24, 129.11, 129.50, 129.82, 130.15, 130.37, 134.25, 134.31, 134.89, 139.93, 140.51, 142.41, 144.05, 144.67; ^{19}F NMR: δ − 62.41 (s, 18F,5,10, 15-*p*-CF$_3$, Ph). HRMS (ESI): M$^+$ = 1836.2311 (expt), 1836.2282 (calcd for C$_{80}$H$_{40}$F$_{18}$N$_8$Os$_2$). Elemental analysis (%): found C 51.99, H 2.72, N 5.34; calcd C 52.34, H 2.20, N 6.10.

{Os[TPC]}₂. Yield 29.5 mg (0.02 mmol, 38.0%). UV−vis (CH$_2$Cl$_2$) λ_{max} (nm) and ε x 10^{-4} (M^{-1}cm^{-1}): 287 (11.45), 363 (8.20), 405 (11.66), 584 (1.96). ^{1}H NMR (400 MHz, − 20 °C): δ 9.00 (d, 4H, $^3J_{HH}$ = 7.52 Hz, 5,15-*o*1-Ph); 8.82 (d, 2H, $^3J_{HH}$ = 7.52 Hz, 10-*o*1-Ph); 8.65 (bs, 4H, β-H); 8.54 (bs, 4H, β-H); 8.15 (bs, 8H, β-H); 8.04 (t, 4H, $^3J_{HH}$ = 7.52 Hz, 5,15-*m*1-Ph); 7.88 (t, 2H, $^3J_{HH}$ = 7.52 Hz, 10-*m*1-Ph); 7.74 (t, 4H, $^3J_{HH}$ = 6.76 Hz, 5,15-*p*-Ph); 7.68 (t, 2H, $^3J_{HH}$ = 7.52 Hz, 10-*p*-Ph); 7.57 (t, 4H, $^3J_{HH}$ = 7.48 Hz, 5,15-*m*2-Ph); 7.48 (t, 2H, $^3J_{HH}$ = 7.52 Hz, 10-*m*2-Ph); 7.31 (d, 4H, $^3J_{HH}$ = 7.52 Hz, 5,15-*o*2-Ph); 7.12 (d, 2H, $^3J_{HH}$ = 7.52 Hz, 10-*o*2-Ph); ^{13}C NMR (100 MHz,

CD$_2$Cl$_2$): δ 115.75, 124.16, 125.15, 126.57, 127.03, 127.18, 127.43, 127.51, 127.55, 134.82, 139.89, 141.06. HRMS (ESI): M$^+$ = 1428.3063 (expt), 1430.3039 (calcd for C$_{74}$H$_{46}$N$_8$Os$_2$). Elemental analysis (%): found C 61.47, H 3.90, N 7.13; calcd C 62.25, H 3.25, N 7.85.

{Os[TpCH₃PC]}₂. Yield 38.0 mg (0.025 mmol, 46.12%). UV−vis (CH$_2$Cl$_2$) λ_{max} (nm) and ε x 10^{-4} (M^{-1}cm^{-1}): 287 (6.80), 363 (5.24), 407 (7.41), 585 (1.52). ^{1}H NMR (400 MHz, − 20 °C): δ 8.81 (d, 4H, $^3J_{HH}$ = 8.36 Hz, 5,15-*o*1-Ph); 8.62 (d, 2H, $^3J_{HH}$ = 8.36 Hz, 10-*o*1-Ph); 8.49 (bs, 4H, β-H); 8.41 (bs, 4H, β-H); 7.91 (d, 4H, $^3J_{HH}$ = 7.36 Hz, 5,15-*m*1-Ph); 7.85 (bs, 4H, β-H); 7.75 (d, 2H, $^3J_{HH}$ = 8.32 Hz, 10-*m*1-Ph); 7.69 (bs, 4H, β-H); 7.44 (d, 4H, $^3J_{HH}$ = 7.36 Hz, 5,15-*m*2-Ph); 7.35 (d, 2H, $^3J_{HH}$ = 8.36 Hz, 10-*m*2-Ph); 7.17 (d, 4H, $^3J_{HH}$ = 7.36 Hz, 5,15-*o*2-Ph); 6.96 (d, 2H, $^3J_{HH}$ = 8.36 Hz, 10-*o*2-Ph); 2.84 (s, 12H, 5,15-*p*-CH$_3$); 2.76 (s, 6H, 10-*p*-CH$_3$); ^{13}C NMR (100 MHz, CDCl$_3$): δ 19.74, 20.99, 22.25, 23.50, 114.88, 116.58, 119.46, 122.83, 123.84, 124.57, 125.59, 125.98. 127.33, 127.66, 128.88, 133.35, 135.07, 136.79, 137.76, 138.34, 140.19, 141.14, 141.23, 142.08. HRMS (ESI): M$^+$ = 1512.4022 (expt), 1514.3978 (calcd for C$_{80}$H$_{58}$N$_8$Os$_2$). Elemental analysis (%): found C 61.41, H 4.53, N 6.63; calcd C 63.56, H 3.87, N 7.41.

{Os[TpOCH₃PC]}₂. Yield 35.3 mg (0.0219 mmol, 40.31%). UV−vis (CH$_2$Cl$_2$) λ_{max} (nm) and ε x 10^{-4} (M^{-1}cm^{-1}): 286 (9.50), 365 (7.62), 407 (10.31), 585 (1.98). ^{1}H NMR (400 MHz, − 20 °C): δ 8.79 (d, 4H, $^3J_{HH}$ = 7.92 Hz, 5,15-*o*1-Ph); 8.65 (d, 2H, $^3J_{HH}$ = 7.60 Hz, 10-*o*1-Ph); 8.56 (bs, 4H, β-H); 8.46 (bs, 4H, β-H); 7.88 (bs, 4H, β-H); 7.67 (bs, 4H, β-H); 7.61 (d, 4H, $^3J_{HH}$ = 8.32 Hz, 5,15-*m*1-Ph); 7.49 (d, 2H, $^3J_{HH}$ = 8.32 Hz, 10-*m*1-Ph); 7.16 (overlapping doublet, 4H, $^3J_{HH}$ = 7.8 Hz, 5,15-*o*2 and *m*2-Ph); 7.07 (d, 2H, $^3J_{HH}$ = 8.32 Hz, 10-*m*2-Ph); 6.98 (d, 2H, $^3J_{HH}$ = 8.32 Hz, 10-*o*2-Ph); 4.12 (s, 12H, 5,15-*p*-OCH$_3$); 4.09 (s, 6H, 10-*p*-OCH$_3$); ^{13}C NMR (100 MHz, CDCl$_3$): δ 55.64, 55.67, 112.32, 112.52, 112.86, 115.28, 119.89, 123.94, 124.82, 126.47, 132.58, 133.10, 134.99, 135.48, 140.24, 140.82, 142.53, 159.10, 159.28. HRMS (ESI): M$^+$ = 1608.3706 (expt), 1610.3673 (calcd for C$_{80}$H$_{58}$N$_8$O$_6$Os$_2$, major isotopomer). Elemental analysis (%): found C 59.11, H 4.10, N 6.57; calcd C 59.76, H 3.64, N 6.97.

Crystallization and Crystallography. X-ray data were collected on beamline 11.3.1 at the Advanced Light Source of Lawrence Berkeley National Laboratory, Berkeley, California. The samples were mounted on MiTeGen kapton loops and placed in a 100(2) K nitrogen cold stream provided by an Oxford Cryostream 700 Plus low temperature apparatus on the goniometer head of a Bruker D8 diffractometer equipped with an APEXII CCD detector. Diffraction data were collected using synchrotron radiation monochromated with silicon(111) to wavelengths of 0.7749(1), 0.7749(1), and 0.8856(1) Å for {Os[TpCF$_3$C]}$_2$, {Os[TPC]}$_2$, and {Os[TpOMeC]}$_2$, respectively. In each case, an approximate full-sphere of data was collected using 1° ω scans. Absorption corrections were applied with SADABS.[54] The structures were solved by intrinsic phasing methods (SHELXT)[55] and refined by full-matrix least-squares on F^2 (SHELXL-2018).[56] Appropriate scattering factors were applied using the XDISP[57] program within the WinGX suite.[58] Hydrogen atoms were geometrically calculated and refined as riding atoms.

All three compounds displayed some disorder of the corrole substituents, which were modeled with occupancies that were restrained to sum to 1.00. Equivalent atoms were constrained to have equal U$_{ij}$ values. For {Os[TpOMeC]}$_2$ and {Os[TPC]}$_2$, the partial occupancy atoms were refined with isotropic thermal displacement parameters. In all cases, equivalent partial occupancy atoms were restrained to have equal U$_{ij}$ values and equivalent disordered groups were restrained to have equal bond lengths and angles.

Large residual peaks of electron density (∼2.5 e/Å^3) were observed for both {Os[TpCF$_3$C]}$_2$ and {Os[TpOMeC]}$_2$. As these were separated from either an Os center ({Os[TpOMeC]}$_2$) or a second large peak of electron density ({Os[TpCF$_3$C]}$_2$) by approximately 2.22 to 2.26 Å, they were presumed to correspond either to the Os centers in an extremely minor twin component or to extremely minor disorder.

A region of negative electron density (ca. −6.5 e/Å^3) near Os2 in {Os[TPC]}$_2$ suggested that the Os2 center has less than 100% occupancy. The occupancy of Os2 was allowed to freely refine and was refined to a value of approximately 71%. This situation was observed for two different crystals of {Os[TPC]}$_2$. A residual peak of electron density near the Os2 center, when modeled as a partial occupancy Os atom (Os3), refined to an occupancy of 2−4%. Modeling this peak as an alternate Os site, however, reduced the occupancy of Os2 by a similar amount. As the relative occupancy of this Os3 center is so low, we could not definitively determine whether it is an alternate location of the Os2 center; this peak has accordingly been left unassigned in the final model. No attempt was made to reduce the occupancy of the atoms that make up the corrole unit.

Computational Methods. All DFT calculations were carried out with the ADF 2016 program system.[59] Relativistic effects were taken into account with the zeroth-order regular approximation (ZORA) applied as a scalar correction and specially optimized all-electron ZORA STO-TZP basis sets for such calculations. A parallel set of calculations were carried out with the same basis set but with a nonrelativistic Hamiltonian. A variety of exchange-correlation functionals were tested; however, since the results proved largely consistent, the discussion above only refers to the B3LYP-D3 results.

◾ ASSOCIATED CONTENT

Accession Codes

CCDC 1883199−1883201 contain the supplementary crystallographic data for this paper. These data can be obtained free of charge via www.ccdc.cam.ac.uk/data_request/cif, or by emailing data_request@ccdc.cam.ac.uk, or by contacting The Cambridge Crystallographic Data Centre, 12 Union Road, Cambridge CB2 1EZ, UK; fax: +44 1223 336033.

◾ AUTHOR INFORMATION

Corresponding Author

*E-mail: abhik.ghosh@uit.no; Telephone: +47 45476145.

Notes

The authors declare no competing financial interest.

◾ ACKNOWLEDGMENTS

◾ REFERENCES

(1) Cotton, F. A.; Wilkinson, G.; Murillo, C. A.; Bochmann, M. *Advanced Inorganic Chemistry*, 6th ed.; Wiley: New York, 1999; pp 758−775.

(2) Pyykkö, P. Relativistic Effects in Chemistry: More Common Than You Thought. *Annu. Rev. Phys. Chem.* **2012**, *63*, 45−64.

(3) Autschbach, J. Perspective: Relativistic effects. *J. Chem. Phys.* **2012**, *136*, 150902.

(4) Gorin, D. J.; Toste, F. D. Relativistic effects in homogeneous gold catalysis. *Nature* **2007**, *446*, 395−403.

(5) Vicha, J.; Novotny, J.; Straka, M.; Repisky, M.; Ruud, K.; Komorovsky, S.; Marek, R. Structure, solvent, and relativistic effects on the NMR chemical shifts in square-planar transition-metal complexes: assessment of DFT approaches. *Phys. Chem. Chem. Phys.* **2015**, *17*, 24944−24955.

(6) Jerabek, P.; Esch, B. v. d.; Schmidbaur, H.; Schwerdtfeger, P. Influence of Relativistic Effects on Bonding Modes in M(II) Dinuclear Complexes (M = Au, Ag, and Cu). *Inorg. Chem.* **2017**, *56*, 14624−14631.

(7) Alvarez-Thon, L.; David, J.; Arratia-Pérez, R.; Seppelt, K. Ground state of octahedral platinum hexafluoride. *Phys. Rev. A: At., Mol., Opt. Phys.* **2008**, *77*, 034502.

(8) Conradie, J.; Ghosh, A. The Blue−Violet Color of Pentamethylbismuth: A Visible Spin-Orbit Effect. *ChemistryOpen* **2017**, *6*, 15−17.

(9) Ghosh, A.; Conradie, J. The Valence States of Copernicium and Flerovium. *Eur. J. Inorg. Chem.* **2016**, *2016*, 2989−2992.

(10) Demissie, T. B.; Garabato, B. D.; Ruud, K.; Kozlowski, P. M. Mercury Methylation by Cobalt Corrinoids: Relativistic Effects Dictate the Reaction Mechanism. *Angew. Chem., Int. Ed.* **2016**, *55*, 11503−11506.

(11) Demissie, T. B.; Conradie, J.; Vazquez-Lima, H.; Ruud, K.; Ghosh, A. Rare and Nonexistent Nitrosyls: Periodic Trends and Relativistic Effects in Ruthenium and Osmium Porphyrin-Based {MNO}[7] Complexes. *ACS Omega* **2018**, *3*, 10513−10516.

(12) Jérôme, F.; Billier, B.; Barbe, J.-M.; Espinosa, E.; Dahaoui, S.; Lecomte, C.; Guilard, R. Evidence for the Formation of a Ru^{III}−Ru^{III} Bond in a Ruthenium Corrole Homodimer. *Angew. Chem., Int. Ed.* **2000**, *39*, 4051−4053.

(13) Kadish, K. M.; Burdet, F.; Jerome, F.; Barbe, J.-M.; Ou, Z.; Shao, J.; Guilard, R. Synthesis, Physicochemical and Electrochemical Properties of Metal-Metal Bonded Ruthenium Corrole Homodimers. *J. Organomet. Chem.* **2002**, *652*, 69−76.

(14) Simkhovich, L.; Luobeznova, I.; Goldberg, I.; Gross, Z. Mono- and Binuclear Ruthenium Corroles: Synthesis, Spectroscopy, Electrochemistry, and Structural Characterization. *Chem. - Eur. J.* **2003**, *9*, 201−208.

(15) Alemayehu, A. B.; Vazquez-Lima, H.; Gagnon, K. J.; Ghosh, A. Stepwise Deoxygenation of Nitrite as a Route to Two Families of Ruthenium Corroles: Group 8 Periodic Trends and Relativistic Effects. *Inorg. Chem.* **2017**, *56*, 5285−5294.

(16) Alemayehu, A. B.; Gagnon, K. J.; Terner, J.; Ghosh, A. Oxidative Metalation as a Route to Size-Mismatched Macrocyclic Complexes: Osmium Corroles. *Angew. Chem., Int. Ed.* **2014**, *53*, 14411−14414.

(17) Palmer, J. H.; Durrell, A. C.; Gross, Z.; Winkler, J. R.; Gray, H. B. Near-IR Phosphorescence of Iridium(III) Corroles at Ambient Temperature. *J. Am. Chem. Soc.* **2010**, *132*, 9230−9231.

(18) Sinha, W.; Ravotto, L.; Ceroni, P.; Kar, S. NIR-Emissive Iridium(III) Corrole Complexes as Efficient Singlet Oxygen Sensitizers. *Dalton Trans.* **2015**, *44*, 17767−73.

(19) Alemayehu, A. B.; Jae Day, N. U.; Mani, T.; Rudine, A. B.; Thomas, K. E.; Gederaas, O. A.; Vinogradov, S. A.; Wamser, C. C.; Ghosh, A. Gold Tris(carboxyphenyl)corroles as Multifunctional Materials: Room Temperature Near-IR Phosphorescence and Applications to Photodynamic Therapy and Dye-Sensitized Solar Cells. *ACS Appl. Mater. Interfaces* **2016**, *8*, 18935−18942.

(20) Lemon, C. M.; Powers, D. C.; Brothers, P. J.; Nocera, D. G. Gold Corroles as Near-IR Phosphors for Oxygen Sensing. *Inorg. Chem.* **2017**, *56*, 10991−10997.

(21) Alemayehu, A. B.; McCormick, L. J.; Gagnon, K. J.; Borisov, S. M.; Ghosh, A. Stable Platinum(IV) Corroles: Synthesis, Molecular Structure, and Room-Temperature Near-IR Phosphorescence. *ACS Omega* **2018**, *3*, 9360−9368.

(22) Borisov, S. M.; Alemayehu, A.; Ghosh, A. Osmium-Nitrido Corroles as NIR Indicators for Oxygen Sensors and Triplet Sensitizers for Organic Upconversion and Singlet Oxygen Generation. *J. Mater. Chem. C* **2016**, *4*, 5822−5828.

(23) Cotton, F. A. Metal-Metal Bonding in [Re$_2$X$_8$]$^{2-}$ Ions and Other Metal Atom Clusters. *Inorg. Chem.* **1965**, *4*, 334−336.

(24) Collman, J. P.; Barnes, C. E.; Woo, L. K. *Proc. Natl. Acad. Sci. U. S. A.* **1983**, *80*, 7684−7688.

(25) Collman, J. P.; Barnes, C. E.; Swepston, P. N.; Ibers, J. A. Synthesis, proton NMR, and structural characterization of binuclear ruthenium porphyrin dimers. *J. Am. Chem. Soc.* **1984**, *106*, 3500−3510.

(26) Collman, J. P.; Arnold, H. J. Multiple Metal-Metal Bonds in 4d and 5d Metal-Porphyrin Dimers. *Acc. Chem. Res.* **1993**, *26*, 586−592.

(27) The broadness of the *β*-H signals for certain compounds suggests a degenerate dynamic process, most likely involving rotation about the Os−Os bond; in general, these signals sharpened at lower temperatures. Importantly, in each case, we could discern only four distinct *β*-H signals, confirming the preponderance of a single dimer conformation with symmetry-related corrole units.

(28) Becke, A. D. Density-functional exchange-energy approximation with correct asymptotic behavior. *Phys. Rev. A: At., Mol., Opt. Phys.* **1988**, *38*, 3098−3100.

(29) Lee, C.; Yang, W.; Parr, R. G. Development of the Colle-Salvetti correlation-energy formula into a functional of the electron density. *Phys. Rev. B: Condens. Matter Mater. Phys.* **1988**, *37*, 785−789.

(30) Stephens, J.; Devlin, F. J.; Chabalowski, C. F.; Frisch, M. J. Ab Initio Calculation of Vibrational Absorption and Circular Dichroism Spectra Using Density Functional Force Fields. *J. Phys. Chem.* **1994**, *98*, 11623−11627.

(31) Grimme, S.; Antony, J.; Ehrlich, S.; Krieg, H. A Consistent and Accurate *Ab Initio* Parametrization of Density Functional Dispersion Correction (DFT-D) for the 94 Elements H-Pu. *J. Chem. Phys.* 2010, *132*, Art. no. 154104.

(32) van Lenthe, E.; Baerends, E. J.; Snijders, J. G. Relativistic regular two-component Hamiltonians. *J. Chem. Phys.* **1993**, *99*, 4597−4610.

(33) van Lenthe, E.; Baerends, E. J.; Snijders, J. G. Relativistic total energy using regular approximations. *J. Chem. Phys.* **1994**, *101*, 9783−9792.

(34) Ziegler, T. Theoretical study of the triple metal bond in d³-d³ binuclear complexes of chromium, molybdenum, tungsten by the Hartree-Fock-Slater transition state method. *J. Am. Chem. Soc.* **1983**, *105*, 7543−7549.

(35) Ziegler, T. Theoretical study of multiple metal-metal bonds in binuclear complexes of Group 6d and Group 7d transition elements with the general formula $M_2Cl_4(PH_3)_4{}^{n+}$ (n = 0, 1, 2) by the Hartree-Fock-Slater transition-state method. *J. Am. Chem. Soc.* **1984**, *106*, 5901−5908.

(36) Ziegler, T. Theoretical study on the quadruple metal bond in d⁴-d⁴ binuclear tetracarboxylate complexes of chromium, molybdenum, and tungsten by the Hartree-Fock-Slater transition-state method. *J. Am. Chem. Soc.* **1985**, *107*, 4453−4459.

(37) Ponec, R.; Bučinský, L.; Gatti. Relativistic Effects on Metal−Metal Bonding: Comparison of the Performance of ECP and Scalar DKH Description on the Picture of Metal−Metal Bonding in $Re_2Cl_8{}^{2-}$. *J. Chem. Theory Comput.* **2010**, *6*, 3113−3121.

(38) Alemayehu, A. B.; Vazquez-Lima, H.; Gagnon, K. J.; Ghosh, A. Tungsten Biscorroles: New Chiral Sandwich Compounds. *Chem. - Eur. J.* **2016**, *22*, 6914−6920.

(39) Alemayehu, A.; Vazquez-Lima, H.; McCormick, L. J.; Ghosh, A. Relativistic effects in metallocorroles: comparison of molybdenum and tungsten biscorroles. *Chem. Commun.* **2017**, *53*, 5830−5833.

(40) Schies, C.; Alemayehu, A. B.; Vazquez-Lima, H.; Thomas, K. E.; Bruhn, T.; Bringmann, G.; Ghosh, A. Metallocorroles as inherently chiral chromophores: resolution and electronic circular dichroism spectroscopy of a tungsten biscorrole. *Chem. Commun.* **2017**, *53*, 6121−6124.

(41) Ghosh, A. Electronic Structure of Corrole Derivatives: Insights from Molecular Structures, Spectroscopy, Electrochemistry, and Quantum Chemical Calculations. *Chem. Rev.* **2017**, *117*, 3798−3881.

(42) Johansen, I.; Norheim, H.-K.; Larsen, S.; Alemayehu, A. B.; Conradie, J.; Ghosh, A. Substituent Effects on Metallocorrole Spectra: Insights from Chromium-Oxo and Molybdenum-Oxo Triarylcorroles. *J. Porphyrins Phthalocyanines* **2011**, *15*, 1335−1344.

(43) Alemayehu, A. B.; Vazquez-Lima, H.; Gagnon, K. J.; Ghosh, A. Stepwise Deoxygenation of Nitrite as a Route to Two Families of

Ruthenium Corroles: Group 8 Periodic Trends and Relativistic Effects. *Inorg. Chem.* **2017**, *56*, 5285−5294.

(44) Einrem, R. F.; Gagnon, K. J.; Alemayehu, A. B.; Ghosh, A. Metal-Ligand Misfits: Facile Access to Rhenium-Oxo Corroles by Oxidative Metalation. *Chem. - Eur. J.* **2016**, *22*, 517−520.

(45) Alemayehu, A. B.; Vazquez-Lima, H.; Beavers, C. M.; Gagnon, K. J.; Bendix, J.; Ghosh, A. Platinum Corroles. *Chem. Commun.* **2014**, *50*, 11093−11096.

(46) Alemayehu, A. B.; Ghosh, A. Gold Corroles. *J. Porphyrins Phthalocyanines* **2011**, *15*, 106−110.

(47) Rabinovich, E.; Goldberg, I.; Gross, Z. Gold(I) and Gold(III) Corroles. *Chem. - Eur. J.* **2011**, *17*, 12294−12301.

(48) Thomas, K. E.; Alemayehu, A. B.; Conradie, J.; Beavers, C.; Ghosh, A. Synthesis and Molecular Structure of Gold Triarylcorroles. *Inorg. Chem.* **2011**, *50*, 12844−12851.

(49) Thomas, K. E.; Vazquez-Lima, H.; Fang, Y.; Song, Y.; Gagnon, K. J.; Beavers, C. M.; Kadish, K. M.; Ghosh, A. Ligand Noninnocence in Coinage Metal Corroles: A Silver Knife-Edge. *Chem. - Eur. J.* **2015**, *21*, 16839−16847.

(50) Gouterman, M.; Wagniére, G. H.; Snyder, L. C. Spectra of Porphyrins. Part II. Four-Orbital Model. *J. Mol. Spectrosc.* **1963**, *11*, 108−115.

(51) Gouterman, M. Optical Spectra and Electronic Structure of Porphyrins and Related Rings. In *The Porphyrins*; Dolphin, D., Ed.; Academic Press: New York, 1978; Vol. *III*, Part A, pp 1−165.

(52) Koszarna, B.; Gryko, D. T. Efficient Synthesis of *meso*-Substituted Corroles in a H_2O−MeOH Mixture. *J. Org. Chem.* **2006**, *71*, 3707−3717.

(53) Many metalloporphyrins and metallocorroles, in particular hemes and Mn and Fe corroles, do not yield satisfactory elemental analyses. Others, such as coinage metal corroles, do so readily. The present complexes turned out to be intermediate. Although the majority of analyses proved to be within 0.5% of their theoretical values, a few exhibited errors of 1−2%. Although the latter can be accounted for by assuming tightly held solvent molecules, the theoretical analyses quoted here refer to simply the solvent-free molecular formulas.

(54) Krause, L.; Herbst-Irmer, R.; Sheldrick, G. M.; Stalke, D. Comparison of silver and molybdenum microfocus X-ray sources for single-crystal structure determination. *J. Appl. Crystallogr.* **2015**, *48*, 3−10.

(55) Sheldrick, G. M. SHELXT - Integrated Space-Group and Crystal-Structure Determination. *Acta Crystallogr., Sect. A: Found. Adv.* **2015**, *A71*, 3−8.

(56) Sheldrick, G. M. Crystal Structure Refinement with SHELXL. *Acta Crystallogr., Sect. C: Struct. Chem.* **2015**, *C71*, 3−8.

(57) Kissel, L.; Pratt, R. H. Corrections to tabulated anomalous-scattering factors. *Acta Crystallogr., Sect. A: Found. Crystallogr.* **1990**, *A46*, 170−175.

(58) Farrugia, L. J. WinGX and ORTEP for Windows: an update. *J. Appl. Crystallogr.* **2012**, *45*, 849−854.

(59) Velde, G. T.; Bickelhaupt, F. M.; Baerends, E. J.; Guerra, C. F.; van Gisbergen, S. J. A.; Snijders, J. G.; Ziegler, T. *J. Comput. Chem.* **2001**, *22*, 931−967.